



RESEARCH

Open Access



Realization of high aspect ratio metalenses by facile nanoimprint lithography using water-soluble stamps

Hojung Choi^{1†}, Joohoon Kim^{2†} , Wonjoong Kim¹, Junhwa Seong², Chanwoong Park¹, Minseok Choi², Nakhyun Kim¹, Jisung Ha¹, Cheng-Wei Qiu³, Junsuk Rho^{2,4,5,6*}  and Heon Lee^{1,7*}

[†]Hojung Choi and Joohoon Kim contributed equally to this work.

*Correspondence: jsrho@postech.ac.kr; heonlee@korea.ac.kr

¹ Department of Materials Science and Engineering, Korea University, Seoul 02841, Republic of Korea

² Department of Mechanical Engineering, Pohang University of Science and Technology (POSTECH), Pohang 37673, Republic of Korea

³ Department of Electrical and Computer Engineering, National University of Singapore, Singapore 117583, Singapore

⁴ Department of Chemical Engineering, Pohang University of Science and Technology (POSTECH), Pohang 37673, Republic of Korea

⁵ POSCO-POSTECH-RIST Convergence Research Center for Flat Optics and Metaphotonics, Pohang 37673, Republic of Korea

⁶ National Institute of Nanomaterials Technology (NINT), Pohang 37673, Republic of Korea

⁷ ZERC, Seoul 02841, Republic of Korea

Abstract

Nanoimprint lithography (NIL) has attracted attention recently as a promising fabrication method for dielectric metalenses owing to its low cost and high throughput, however, high aspect ratio (HAR) nanostructures are required to manipulate the full 2π phase of light. Conventional NIL using a hard-polydimethylsiloxane (h-PDMS) mold inevitably incurs shear stress on the nanostructures which is inversely proportional to the surface area parallel to the direction of detachment. Therefore, HAR structures are subjected to larger shear stresses, causing structural failure. Herein, we propose a novel wet etching NIL method with no detachment process to fabricate flawless HAR metalenses. The water-soluble replica mold is fabricated with polyvinyl alcohol (PVA) which is simpler than an h-PDMS mold, and the flexibility of the PVA mold is suitable for direct printing as its high tensile modulus allows high-resolution patterning of HAR metalenses. The diffraction-limited focusing of the printed metalenses demonstrates that it operates as an ideal lens in the visible regime. This method can potentially be used for manufacturing various nanophotonic devices that require HAR nanostructures at low cost and high throughput, facilitating commercialization.

Keywords: Nanoimprint lithography, Wet etching, Polyvinyl alcohol, High fidelity nanofabrication, High aspect ratio nanostructure, Metalens

Introduction

High aspect ratio (HAR) structures have been employed in various applications including biological sensing [1–4], plasmonic resonators [5–10], and nanophotonic devices [11–13]. These structures exhibit unusual physical properties compared to that of their bulk form owing to their unique features such as height, sharpness, and topology of HAR structures. Metasurfaces made up of an array of subwavelength nanoantennas can modulate the wavefront of light in the desired manner. Their 2-dimensional nature significantly reduces the thickness of optical devices and allows for the development of flat optics [14–26]. Plasmonic metasurfaces composed of metallic nanoantennas provide complete 2π phase control by the resonance of nanoantennas [27], but are limited by the intrinsic ohmic loss of metal. Therefore,

dielectric materials have been exploited to increase the efficiency of metasurfaces up to 80% [24, 28, 29], while nanoparticle embedded resin (PER) has been proven for measured efficiencies over 95% [30]. Unlike metals, dielectric metasurfaces require HAR nanoantennas to control the full 2π phase of light. Accordingly, the fabrication process of HAR structures is an important consideration for high efficiency metasurfaces.

Electron-beam lithography (EBL) is mainly used for the fabrication of HAR metalenses owing to its high resolution [31], but it has limitations such as high cost and low throughput. Nanoimprint lithography (NIL) is receiving considerable attention as an alternative to EBL for metasurface manufacturing, using elastomeric stamps containing nanoscale templates [32–36]. Although EBL is still used to produce the master stamp for NIL, once the master stamp is produced, the replica mold can be created quickly and repeatedly at a low cost, and can itself be used as a metalens. NIL significantly reduces the manufacturing cost of metalenses; however, it requires secondary operations, including deposition of high refractive index materials such as TiO_2 and GaN, and HAR etching to create vertical structures [32, 33]. The metalenses fabricated via secondary operations exhibit a tapered or cone-shaped meta-atom owing to difficulties in vertical etching. Therefore, previous studies have developed the concept of PER for the single-step manufacturing of dielectric metalenses without any secondary operations [37–39]. However, PER-based manufacturing is limited due to low aspect ratio nanostructures, small patterning areas, and low yield. This is because the fabrication process of the PER pattern involves detaching the hard-PDMS (h-PDMS) replica mold from the substrate. At this stage, shear stress is inevitably applied to the nanostructures which tend to bend or break in the direction of the applied force, deteriorating the quality of the device. Moreover, manufacturing HAR metalenses comprised of PER meta-atoms is even more challenging as the amount of shear stress is inversely proportional to the surface area in the parallel direction. Therefore, HAR structures are subjected to even larger stresses. This large shear stress in HAR structures incur the breakage and collapse of replicated patterns in the direction of the force applied during the detachment (Supplementary Note 1) [40, 41].

Herein, we propose a new NIL method for the centimeter-scale fabrication of flawless HAR metalenses consisting of PER. To mitigate the warpage and breakage of the nanostructures during mold detachment, we eliminate the detaching process and replace it with wet etching of a replica mold made of a water-soluble polymer, polyvinyl alcohol (PVA) [42–44]. It is notable that the proposed water-soluble mold expands the printable area from the micrometer scale to the centimeter scale. The PVA replica mold is flexible and has good contact with the substrate, making it suitable as a mold for direct patterning. It is thick enough for handling as a single layer, thereby eliminating the need for a backbone polymer. In addition, the manufacturing process is simple, and the materials used in the process, including deionized (DI) water, are harmless to the human body. As the last step of NIL, the replica mold made of PVA is completely removed via wet etching with DI water. The wet etching of PVA mold does not exert any external force on the nanostructure, leading to the fabrication of flawless HAR metalenses. The replicated nanopatterns are vertical, with an HAR and the same arrangement and size as the master stamp.

Results and discussion

Characteristics of the PVA replica mold

We prepared a replica mold using PVA and performed UV NIL to fabricate HAR metasurfaces. The PVA replica mold is suitable for sub-100 nm metasurface replication due to its high tensile modulus of 2.936 MPa (Supplementary Note 3). This prevents the “pairing” of lateral collapse with the surrounding structures that occurs at PDMS mold due to its elastomeric characteristic [45, 46]. The PVA mold has a thickness of 78 μm , which is thick enough to handle without any backbone layer (Supplementary Note 4). Therefore, the fabrication process of PVA mold is much simpler than h-PDMS mold which requires PDMS backbone layer since h-PDMS is stiff and thin. Moreover, our PVA mold eliminates the vapor self-assembled monolayer (SAM) coating process required for conventional h-PDMS molds to prevent the pattern sticking during detachment [47]. More than 3 applications of vapor phase SAM coating is required on the mold, making the preparation process longer. However, since our wet etching NIL method does not have detachment, vapor phase SAM coating is not essential on the PVA mold. The fabrication process of PVA mold is described in Supplementary Note 7 and [Methods](#) section.

Metasurface fabrication by wet etching NIL

Metasurfaces require the confinement of light in the nanostructures for the manipulation of its amplitude and phase. Polymeric resins typically used in NIL are not appropriate for metasurface fabrication owing to their low refractive index. In this study, we use TiO_2 PER to enhance the refractive index. Specifically, 30 nm TiO_2 in 30 wt% resin (Supplementary Note 5, 6) is dispersed in a solvent of 4-Methyl-2-pentanone (MIBK) and mixed with photoinitiator 1-Hydroxy-cyclohexyl-phenyl-ketone and dipentaerythritol penta-/hexa-acrylate to obtain TiO_2 PER (Supplementary Note 7).

The characteristics of TiO_2 PER are analyzed via ellipsometry. 89 wt% TiO_2 PER is spin-coated on a silicon substrate and cured with UV illumination to measure the extinction coefficient and refractive index. The refractive index is recorded to be 1.8 over a range of $400 \text{ nm} \leq \lambda \leq 800 \text{ nm}$, strengthening the confinement of light in the PER nanostructures. TiO_2 PER shows an extinction coefficient of ~ 0 because TiO_2 nanoparticle and polymeric resin are both low-loss materials, which increases the conversion efficiency of metalens (Fig. 1a).

A fabrication process of wet etching NIL is shown in Fig. 1b. TiO_2 PER is dropped on the PVA replica mold and spin-coated at 3000 rpm for 30 s to form a uniform layer of TiO_2 PER. A TiO_2 spin-coated PVA mold is covered on the substrate, and a pressure of 5 bar is applied with UV exposure for 40 min. After PER is cured by sufficient pressure and UV illumination, the substrate attached to the PVA mold is immersed in DI water for 4 h. As PVA is a water-soluble polymer, the PVA mold covering the substrate dissolves, and only the replicated TiO_2 nanostructures remain on the substrate.

Unlike conventional NIL, which inevitably introduces shear stress in cured nanostructures, the developed wet etching NIL method can replicate various patterns without faults. Figure 1c-h show SEM images of various replicated patterns using the PVA replica mold. Patterns of various shapes and sizes, such as nanopillars (Fig. 1c, d), nanocones (Fig. 1e), and nanoline (Fig. 1f, g) are successfully replicated. Notably,

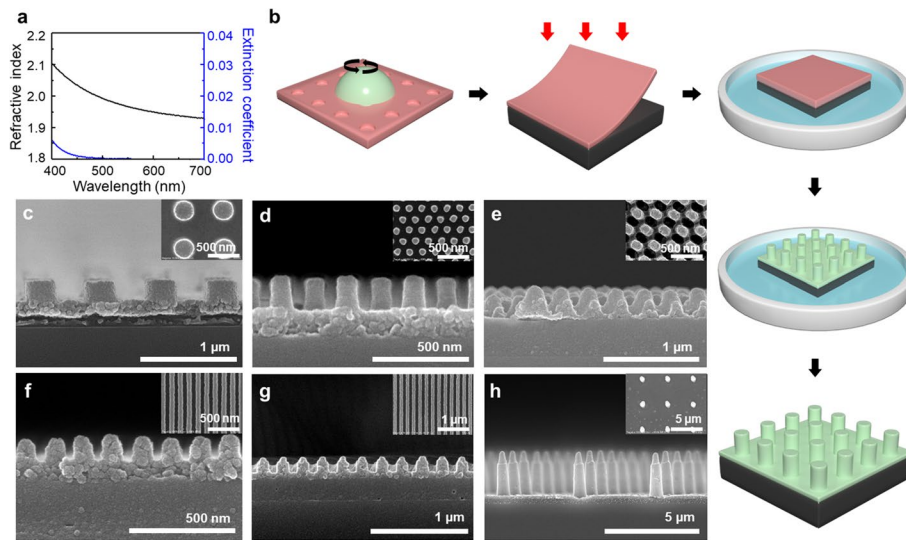


Fig. 1 Wet etching nanoimprint lithography using the PVA replica mold. **a** Ellipsometry analysis of TiO_2 89 wt% PER. **b** Schematic of the wet etching NIL process. **c–h** Scanning electron microscopy (SEM) images of various replicated nanopatterns using PVA replica mold. Nanopillar: **c** Square array, Diameter (D) = 200 nm, Period (P) = 400 nm, Height (H) = 200 nm, Aspect Ratio (AR , H/D) = 1, **d** Hexagonal array, D = 100 nm, P = 200 nm, H = 200 nm, AR = 2. Densely packed nanocone: **e** Hexagonal array, D = 300 nm, P = 300 nm, H = 150 nm. Nanoline: **f** D = 70 nm, P = 140 nm, H = 70 nm, **g** D = 100 nm, P = 200 nm, H = 100 nm. High aspect ratio pillar: **h** Square array, D = 500 nm, P = 2 μm , H = 3 μm , AR = 6

even HAR pillar patterns (Fig. 1h, aspect ratio (AR) = 6) that are difficult to replicate with PDMS (Supplementary Note 1a) show high fidelity.

Design and simulation of HAR metalens

The anisotropic meta-atom is finely designed to manipulate the phase of the incident light using the concept of Pancharatnam–Berry (PB) phase (Fig. 2a). The designed meta-atom functions as a half-wave plate; therefore, a full 2π phase modulation can be attained by rotation of anisotropic meta-atom. The ideal meta-atom using the PB phase has a π phase difference between the x - and y - components of the electric fields. We use rigorous coupled-wave analysis (RCWA) to calculate the optical characteristics of the anisotropic meta-atom. Conversion efficiencies are calculated at the wavelength $\lambda = 532$ nm by varying the parameters of the meta-atom—length (250–400 nm), width (50–200 nm), with a fixed height (700 nm) and period (450 nm) (Fig. 2b). We confirm that the meta-atom with a length 310 nm and width 120 nm has a conversion efficiency of 64% and a near- π phase difference between the x - and y - components of the electric fields (Fig. 2c). Moreover, the designed meta-atom can function at other wavelengths in the visible regime due to the broadband property of the PB phase (Fig. 2d). The designed meta-atom has conversion efficiencies of 48% at $\lambda = 450$ nm and 27% at $\lambda = 635$ nm.

Using the designed meta-atom, a metalens is designed to follow a quadratic phase distribution to focus the cross-polarized light and the expression of the phase distribution is indicated as follows,

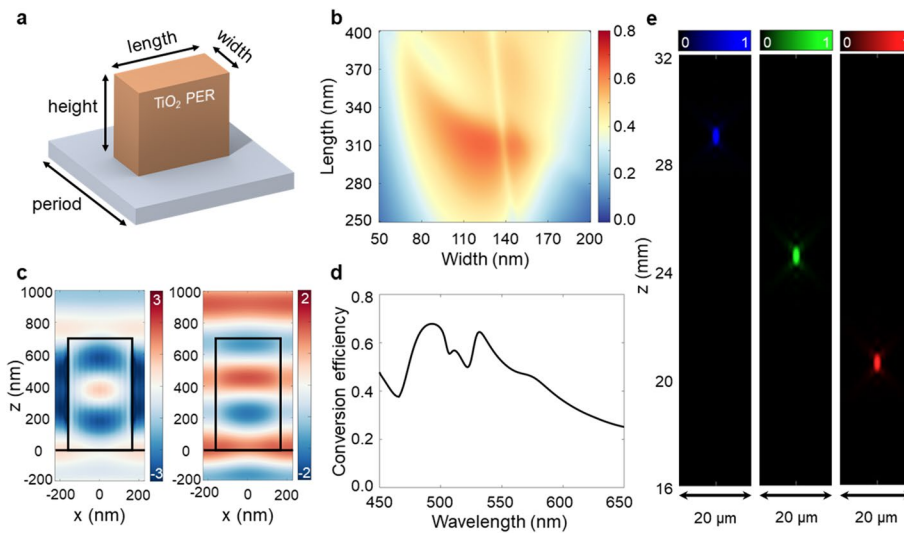


Fig. 2 Design and simulation of metalens. **a** Schematic of anisotropic meta-atom. **b** Simulated conversion efficiencies of meta-atoms at $\lambda = 532$ nm. (height = 700 nm, period = 450 nm) **c** Real part of electric field in designed meta-atom: x-component (left) and y-component (right). **d** Plot of conversion efficiencies in the visible wavelength range. **e** Simulated optical field based on the Rayleigh–Sommerfeld diffraction formula at wavelength of 450 nm (left), 532 nm (center), and 635 nm (right)

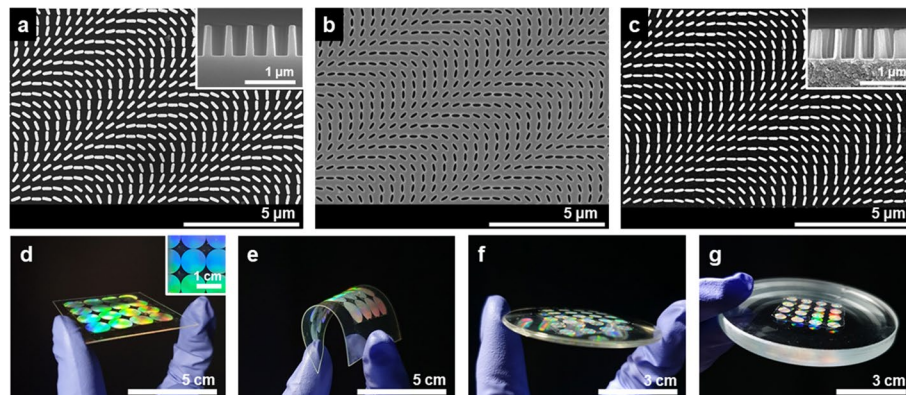


Fig. 3 **a–c** SEM images of HAR-metalens. **a** Master stamp of the metalens (Length = 320 nm, Width = 120 nm, Height = 700 nm, Aspect Ratio (H/W) = 5.8). **b** PVA replica mold. **c** Replicated metalens. **d–g** Photographs of printed 10 mm metalenses on various substrates: **(d)** glass substrate; **(e)** flexible polyethylene terephthalate (PET) film; **(f)** convex substrate; and **(g)** concave substrate

$$\varphi(x, y) = -\frac{2\pi}{\lambda} \left(\sqrt{x^2 + y^2 + f^2} - f \right) \quad (1)$$

where $\lambda = 532$ nm is a target wavelength, f is the designed focal length, and x and y are coordinates of each meta-atom. The focusing properties of the designed metalens are simulated using the Rayleigh–Sommerfeld diffraction formula [48]. The simulated focal lengths of the designed metalens are 2.45 cm at 532 nm, 2.90 cm at 450 nm, and 2.05 cm at 635 nm, owing to chromatic aberration. The corresponding numerical apertures are 0.2 at 532 nm, 0.17 at 450 nm, and 0.24 at 635 nm.

Fabricated HAR-metalens via wet etching NIL

Figure 3a-c show SEM images of HAR metalens. The master stamp is fabricated via photolithography (Fig. 3a) [49]. The meta-atom is 320 nm in length, 120 nm wide, and 700 nm in height, with an aspect ratio (H/W) 5.8. The replica mold of the master stamp is fabricated with PVA resin (Fig. 3b), and TiO₂ PER nanostructures are replicated through wet etching UV NIL (Fig. 3c). Although the printed metalenses have a residual layer, the efficiency is maintained with residual layers around 100 nm, which is the measured thickness of the residual layer (Supplementary Note 2). This is because the residual layer can increase transmission by acting as an antireflection layer. Moreover, the scattering effect of TiO₂ nanoparticles is negligible since nanoparticles have a small diameter of 30 nm (Supplementary Note 5) [30]. The PVA mold has a tensile modulus of 2.936 MPa, 1.6 times higher than commonly used PDMS, preventing sagging and pairing (Supplementary Note 3) [50]. The final PER nanostructures, replicated with the same configuration as the master stamp, exhibit the excellent resolution of the PVA mold. Our wet etching NIL method replicates HAR patterns with vertical features that are identical to the master stamp as shown in the inset of Fig. 3c. This method does not require secondary operations and the materials used in the process such as DI water and PVA are harmless to the human body.

Optical properties of the metalens

A customized measurement setup is used to measure the optical characteristics of fabricated metalenses (Supplementary Note 8). The normalized intensity profiles of the focal spot are measured at different wavelengths of 450 nm, 532 nm, and 635 nm and plotted in Fig. 4a-c. Moreover, the intensity distributions of the focal point are compared with ideal diffraction-limited Airy disks at three different wavelengths (Fig. 4d-f). The measured intensity distributions agree closely with the ideal Airy disk at each wavelength, indicating that the fabricated metalenses act as a perfect lens. The measured focusing

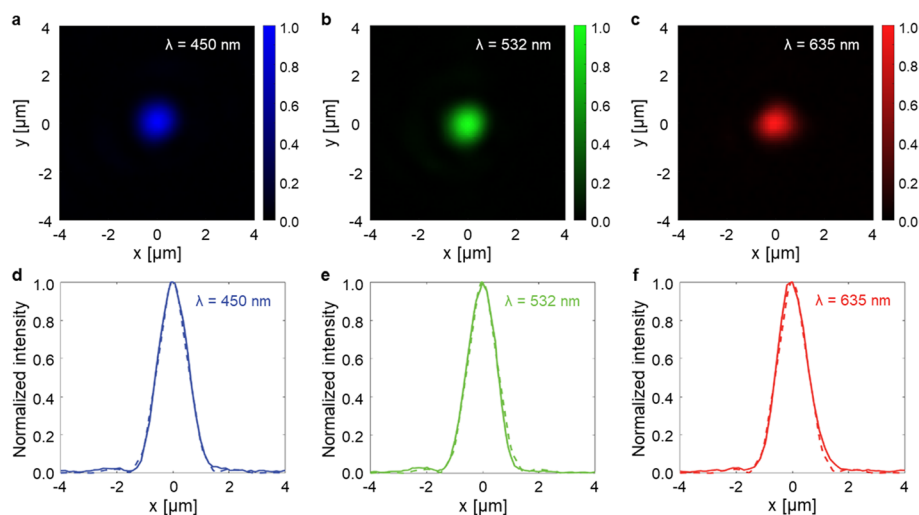


Fig. 4 Optical characterization. **a-c** Measured normalized intensity distributions of the focal planes at (a) 450 nm, (b) 532 nm, and (c) 635 nm. **d-f** Focusing intensity distribution with ideal Airy disks at (d) 450 nm, (e) 532 nm, and (f) 635 nm

efficiencies of the fabricated metalenses are 24% at $\lambda = 450$ nm, 45% at $\lambda = 532$ nm, 14% at $\lambda = 635$ nm. The measured efficiencies of fabricated metalenses are lower than the simulated results owing to fabrication defects. These can be improved by optimizing the fabrication process.

Conclusion

In this study, we developed a wet etching NIL method to fabricate perfect HAR metalenses without defects. The main advantages of our method are the facile fabrication process of PVA mold compared to methods of previous studies using h-PDMS mold and large area fabrication with high pattern resolution comparable to conventional metalens fabrication using electron-beam lithography. Notably, we fabricated centimeter-scale PER metalenses for the first time. The PVA replica mold used in this method is water-soluble and can be wet-etched in DI water, which eliminates the detachment process. As wet etching of the mold does not lead to the application of external forces to the cured nanostructures, the metalenses fabricated using this method are composed of unbroken, vertical, HAR meta-atoms that perfectly mimic patterns of the master stamp. The flexibility of the PVA mold enables direct patterning on various substrates, including glass, flexible films, and curved substrates. As a proof of concept, a 10 mm diameter HAR metalens array was fabricated using the PVA replica mold. The fabricated HAR metalenses exhibit diffraction-limited focusing and a measured focusing efficiency of 28% at 532 nm, which can be improved by optimization of the fabrication process. Moreover, as the PVA mold used in this method can act as a replica mold of imprinting, it can be applied in various ways throughout the imprinting process. Although TiO_2 PER was developed in previous work, large-area patterning of TiO_2 PER metasurfaces has been challenging for a long time. It is notable that centimeter-scale patterning is achieved without defects in this work. Although the PVA mold is not reusable, it can be easily fabricated repeatably from the master stamp and has powerful advantage that enables large-area patterning of TiO_2 PER. Moreover, metalenses can be fabricated not only with TiO_2 PER, which is used in this study, but also with other high refractive index PERs such as Si and GaN. We strongly believe that the method developed in this study facilitate commercialization of metasurface fabrication with defect-free HAR nanostructures via NIL.

Methods

Preparation of master stamp

A master stamp was fabricated by patterning metalenses using photolithography on a silicon substrate [49]. High-power electron-beam lithography was used to fabricate the reticle using a positive photoresist (FEP series, Fujifilm Ltd.) and developer (tetramethylammonium: TMAH). Molybdenum silicide layer was deposited using an electron-beam evaporator to form the block layer in the reticle. Using the argon fluoride (ArF) photolithography, the reticle pattern was transferred onto a positive-tone photoresist using ArF lithography and developer (TMAH). By using the patterned photoresist as an etching mask, the master stamp was fabricated with ICP dry etcher.

SAM coating was applied to the master stamp to lower the surface energy to facilitate the separation of the mold. SAM is a 2-dimensional molecular assemblies formed on a solid surface by the adsorption and organization of an active surfactant. The driving

force for spontaneous SAM formation is the chemical bond synthesis by intermolecular interactions between the substrate surface and surfactant molecules [51, 52].

A fluorine-based SAM solution was prepared by mixing heptadecafluoro-1,1,2,2-tetrahydrodecyltricholasilane (HDFS) and hexane in a 1:1000 ratio for 10 min. Then the master stamp, which was pre-treated with UV ozone, was immersed in the SAM solution for 10 min. The SAM solution was completely removed by rinsing the master stamp with hexane and DI water. The SAM formed through this process facilitates the separation of the PVA mold by moderating the surface energy of the master stamp.

Fabrication of PVA replica mold

The PVA resin for the PVA replica mold is prepared by placing PVA pellets (Sigma Aldrich, Poly(vinyl alcohol), 96% hydrolyzed, Mw 85,000–124,000) in DI water and completely dissolving them by stirring at 90 °C for 24 h. Subsequently, 5 wt% PVA resin is poured onto the SAM-coated master stamp. Pores in the PVA resin are removed in a vacuum using a desiccator. After drying the resin at 30 °C for 24 h, a uniform PVA layer without pores is formed on the master stamp. By separating the PVA layer from the master stamp, the PVA replica mold is obtained. Separation of PVA from the master stamp is easy owing to the flexibility of the PVA mold.

Formulation of TiO₂ PER

We prepared TiO₂ 30 wt% resin (Ditto Technology) where TiO₂ NPs (30 nm size, anatase) were dispersed in a solvent of 4-Methyl-2-pentanone (MIBK). Then we mixed TiO₂ 30 wt% resin with 1-Hydroxy-cyclohexyl-phenyl-ketone (Sigma Aldrich) as a photoinitiator, dipentaerythritol penta-/hexa-acrylate (Sigma Aldrich) as a polymer matrix, and additional solvent of MIBK (Sigma Aldrich). The mixture of TiO₂ NPs, photoinitiator, polymer matrix and solvent has 89 wt% TiO₂ and we called this resin as TiO₂ PER in this work.

Spin-coating of TiO₂ PER on PVA replica mold

As a previous step in imprinting, we spin-coated TiO₂ PER on PVA replica mold. We attached PVA replica mold to the substrate by using ketone tape and drop TiO₂ PER on PVA mold, where TiO₂ PER have been pre-sonicated 10 min for dispersion. Then we spin-coated TiO₂ PER in 3000 rpm for 30 s to form thin layer on PVA replica mold.

UV Imprinting and wet etching process

UV-ozone was pre-treated on the substrate for 3 min, and the spin-coated PVA mold was attached to the pre-treated substrate. We applied pressure of 5 bar and UV illumination (365 nm, 1W) for 40 min to cure the TiO₂ PER. After the imprinting process, we put the substrate which was covered with PVA mold in DI water (30 °C, 200 mL in petri dish) for 2 h. To prevent the evaporation of the DI water, we sealed the petri dish with plastic wrap during the dissolution of PVA. As the PVA mold dissolved, we took the substrate out of the water where the PVA mold had eliminated. Then we performed DI water cleaning process once, and blew out the remaining DI water from the substrate by N₂ blowing in room temperature.

Abbreviations

HAR	High aspect ratio
NIL	Nanoimprint lithography
h-PDMS	Hard-polydimethylsiloxane
PVA	Polyvinyl alcohol
EBL	Electron-beam lithography
ArF	Argon fluoride
DI	Deionized
SAM	Self-assembled monolayer
MIBK	4-Methyl-2-pentanone
PER	Particle embedded resin
PB	Pancharatnam–Berry
HDFS	Heptadecafluoro-1,1,2,2-tetra-hydrodecyltricholasilane
RCWA	Rigorous coupled-wave analysis

Supplementary Information

The online version contains supplementary material available at <https://doi.org/10.1186/s43074-023-00096-2>.

Additional file 1: Supplementary Note 1. Replicated HAR nanostructures via PDMS and PVA mold. **Supplementary Note 2.** Calculated conversion efficiency by varying residual layer thickness. **Supplementary Note 3.** Tensile modulus of PVA mold. **Supplementary Note 4.** Characteristics of PVA replica mold. **Supplementary Note 5.** Size distribution of TiO₂ PER. **Supplementary Note 6.** Nanoindentation test on TiO₂ PER thin film. **Supplementary Note 7.** Fabrication process of PVA replica mold. **Supplementary Note 8.** Optical setup to characterize the focal spot of metalens.

Acknowledgements

Argon fluoride photolithography and electron-beam lithography were done in National Nano Fab Center (NNFC) and National Institute of Nanomaterials Technology (NINT), respectively, both user facilities supported by the Korean government.

Authors' contributions

J.R. and H.L. conceived the idea and initiated the project. J.K. and W.K. designed and fabricated the master stamps. H.C., C.P., N.K. and J.H. developed the PVA mold replication and imprinting processes. J.K. performed the simulations. J.K., J.S. and M.C. conducted optical characterizations of metalens. C.-W.Q. supported the materials characterizations. H.C. and J.K. wrote the manuscript. All authors confirmed the final manuscript. J.R. and H.L. guided the entire work.

Funding

H.L. acknowledges the Technology Innovation program (20016234) funded by the Ministry of Trade and Industry & Energy (MOTIE) and the National Research Foundation (NRF) grants (NRF-2019K1A4A7A02113032, NRF-2022M3H4A1A02046445, NRF-2018M3D1A1058997) funded by the Ministry of Science and ICT (MSIT) of the Korean government. J.R. acknowledges the POSCO-POSTECH-RIST Convergence Research Center program funded by POSCO, an industry-university strategic grant funded by Samsung Display, and the NRF grants (NRF-2022M3C1A3081312, NRF-2022M3H4A1A02074314, NRF-2019R1A5A8080290, CAMM-2019M3A6B3030637) funded by the MSIT of the Korean government. C.W.Q. acknowledges the support by AME Individual Research Grant (IRG) funded by A*STAR, Singapore (Grant No. A2083c0060). J.K. acknowledges the POSTECH Alchemist fellowship.

Availability of data and materials

The datasets used or analyzed during the current study are available from the corresponding author on reasonable request.

Declarations

Competing interests

The authors declare that they have no competing interests.

Received: 5 December 2022 Revised: 16 May 2023 Accepted: 30 May 2023

Published online: 15 June 2023

References

1. Higgins SG, Becce M, Belessiotis-Richards A, Seong H, Sero JE, Stevens MM. High-aspect-ratio nanostructured surfaces as biological metamaterials. *Adv Mater.* 2020;32:1903862. <https://doi.org/10.1002/adma.201903862>.
2. Chiappini C. Nanoneedle-based sensing in biological systems. *ACS Sens.* 2017;2:1086–102. <https://doi.org/10.1021/acssensors.7b00350>.
3. Mas-Moruno C, Su B, Dalby MJ. Multifunctional coatings and nanotopographies: toward cell instructive and antibacterial implants. *Adv Healthc Mater.* 2019;8:1801103. <https://doi.org/10.1002/adhm.201801103>.

4. Harding FJ, Surdo S, Delalat B, Cozzi C, Elnathan R, Gronthos S, Voelcker NH, Barillaro G. Ordered silicon pillar arrays prepared by electrochemical micromachining: substrates for high-efficiency cell transfection. *ACS Appl Mater Interfaces*. 2016;8:29197–202. <https://doi.org/10.1021/acsami.6b07850>.
5. Päivänranta B, Merbold H, Giannini R, Büchi L, Gorelick S, David C, Löffler JF, Feurer T, Ekinici Y. High aspect ratio plasmonic nanostructures for sensing applications. *ACS Nano*. 2011;5:6374–82. <https://doi.org/10.1021/nn201529x>.
6. Koenderink AF. Plasmon nanoparticle array waveguides for single photon and single plasmon sources. *Nano Lett*. 2009;9:4228–33. <https://doi.org/10.1021/nl902439n>.
7. McFarland AD, Van Duyne RP. Single silver nanoparticles as real-time optical sensors with zeptomole sensitivity. *Nano Lett*. 2003;3:1057–62. <https://doi.org/10.1021/nl034372s>.
8. Lyvers DP, Moon JM, Kildishev AV, Shalaev VM, Wei A. Gold Nanorod arrays as plasmonic cavity resonators. *ACS Nano*. 2008;2:2569–76. <https://doi.org/10.1021/nn8006477>.
9. McPhillips J, Murphy A, Jonsson MP, Hendren WR, Atkinson R, Höök F, Zayats AV, Pollard RJ. High-performance biosensing using arrays of plasmonic nanotubes. *ACS Nano*. 2010;4:2210–6. <https://doi.org/10.1021/nn9015828>.
10. Carstensen MS, Zhu X, Iyore OE, Mortensen NA, Levy U, Kristensen A. Holographic resonant laser printing of metasurfaces using plasmonic template. *ACS Photonics*. 2018;5:1665–70. <https://pubs.acs.org/doi/full/10.1021/acsp Photonics.7b01358>.
11. Khorasaninejad M, Chen WT, Devlin RC, Oh J, Zhu AY, Capasso F. Metalenses at visible wavelengths: diffraction-limited focusing and subwavelength resolution imaging. *Science*. 2016;352:1190–4. <https://www.science.org/doi/10.1126/science.aaf6644>.
12. Ren H, Fang X, Jang J, Bürger J, Rho J, Maier SA. Complex-amplitude metasurface-based orbital angular momentum holography in momentum space. *Nat Nanotechnol*. 2020;15:948–55. <https://doi.org/10.1038/s41565-020-0768-4>.
13. Chen WT, Zhu AY, Sanjeev V, Khorasaninejad M, Shi Z, Lee E, Capasso FA. Broadband achromatic metalens for focusing and imaging in the visible. *Nat Nanotechnol*. 2018;13:220–6. <https://doi.org/10.1038/s41565-017-0034-6>.
14. Jung C, Kim G, Jeong M, Jang J, Dong Z, Badloe T, Yang JKW, Rho J. Metasurface-driven optically variable devices. *Chem Rev*. 2021;121:13013–50. <https://doi.org/10.1021/acs.chemrev.1c00294>.
15. Hu J, Bandyopadhyay S, Liu YH, Shao LY. A Review on Metasurface: From Principle to Smart Metadevices. *Front Phys*. 2021;8:586087. <https://doi.org/10.3389/fphy.2020.586087>.
16. Arbabi A, Arbabi E, Horie Y, Kamali SM, Faraon A. Planar metasurface retroreflector. *Nat Photonics*. 2017;11:415–20. <https://doi.org/10.1038/nphoton.2017.96>.
17. Zheng G, Mühlenbernd H, Kenney M, Li G, Zentgraf T, Zhang S. Metasurface holograms reaching 80% efficiency. *Nat Nanotechnol*. 2015;10:308–12. <https://doi.org/10.1038/nnano.2015.2>.
18. Yu N, Capasso F. Flat optics with designer metasurfaces. *Nat Mater*. 2014;13:139–50. <https://doi.org/10.1038/nmat3839>.
19. Kim J, Jeon D, Seong J, Badloe T, Jeon N, Kim G, Kim J, Baek S, Lee JL, Rho J. Photonic encryption platform via dual-band vectorial metaholograms in the ultraviolet and visible. *ACS Nano*. 2022;16:3546–53. <https://doi.org/10.1021/acsnano.1c10100>.
20. Badloe T, Kim J, Kim I, Kim WS, Kim YK, Rho J. Liquid crystal-powered mie resonators for electrically tunable photorealistic color gradients and dark blacks. *Light Sci Appl*. 2022;11:1–11. <https://doi.org/10.1038/s41377-022-00806-8>.
21. Kim J, Kim W, Oh DK, Kang H, Kim H, Badloe T, Kim S, Park C, Choi H, Lee H, Rho J. One-step printable platform for high-efficiency metasurfaces down to the deep-ultraviolet region. *Light Sci Appl*. 2023;12:68. <https://doi.org/10.1038/s41377-023-01086-6>.
22. Kim J, Yang Y, Badloe T, Kim I, Yoon G, Rho J. Geometric and physical configurations of meta-atoms for advanced metasurface holography. *InfoMat*. 2021;3:739–54. <https://doi.org/10.1002/inf2.12191>.
23. Kim I, Yoon G, Jang J, Genevet P, Nam KT, Rho J. Outfitting next generation displays with optical metasurfaces. *ACS Photonics*. 2018;5:3876–95. <https://doi.org/10.1021/acsp Photonics.8b00809>.
24. Lin D, Fan P, Hasman E, Brongersma ML. Dielectric gradient metasurface optical elements. *Science*. 2014;345:298–302. <https://www.science.org/doi/10.1126/science.1253213>.
25. So S, Kim J, Badloe T, Lee C, Yang Y, Kang H, Rho J. Multicolor and 3D holography generated by inverse-designed single-cell metasurfaces. *Adv Mater*. 2022;27:2208520. <https://doi.org/10.1002/adma.202208520>.
26. Ko B, Badloe T, Yang Y, Park J, Kim J, Jeong H, Jung C, Rho J. Tunable metasurfaces via the humidity responsive swelling of single-step imprinted polyvinyl alcohol nanostructures. *Nat Commun*. 2022;13:6256. <https://doi.org/10.1038/s41467-022-34566-1>.
27. Zhu X, Czolkos I, Johansson A, Nielsen T, Kristensen A. Master origination by 248 nm DUV lithography for plasmonic color generation. *Appl Phys Lett*. 2021;118:141103. <https://doi.org/10.1063/5.0046163>.
28. Yu YF, Zhu AY, Paniagua-Domínguez R, Fu YH, Luk'yanchuk B, Kuznetsov AI. High-Transmission Dielectric Metasurface with 2π Phase Control at Visible Wavelengths. *Laser Photonics Rev*. 2015;9:412–8. <https://doi.org/10.1002/lpor.201500041>.
29. Devlin RC, Khorasaninejad M, Chen WT, Oh J, Capasso F. Broadband high-efficiency dielectric metasurfaces for the visible spectrum. *Proc Natl Acad Sci*. 2016;113:10473–8. <https://doi.org/10.1073/pnas.1611740113>.
30. Kim J, Oh DK, Kim H, Yoon G, Jung C, Kim J, Badloe T, Kang H, Kim S, Yang Y, Lee J, Ko B, Ok JG, Rho J. Metasurface holography reaching the highest efficiency limit in the visible via one-step nanoparticle-embedded-resin printing. *Laser Photonics Rev*. 2022;16:2200098. <https://doi.org/10.1002/lpor.202200098>.
31. Yoon G, Kim I, Rho J. Challenges in fabrication towards realization of practical metamaterials. *Microelectron Eng*. 2016;163:7–20. <https://doi.org/10.1016/j.mee.2016.05.005>.
32. Wu W, Yu Z, Wang SY, Williams RS, Liu Y, Sun C, Zhang X, Kim E, Shen YR, Fang NX. Midinfrared metamaterials fabricated by nanoimprint lithography. *Appl Phys Lett*. 2007;90:063107. <https://doi.org/10.1063/1.2450651>.
33. Chanda D, Shigeta K, Gupta S, Cain T, Carlson A, Mihi A, Baca AJ, Bogart GR, Braun P, Rogers JA. Large-area flexible 3D optical negative index metamaterial formed by nanotransfer printing. *Nat Nanotechnol*. 2011;6:402–7. <https://doi.org/10.1038/nnano.2011.82>.

34. Byeon KJ, Lee H. Recent progress in direct patterning technologies based on nano-imprint lithography. *Eur Phys J Appl Phys*. 2012;59.<https://doi.org/10.1051/EPJAP/2012120166>.
35. Hong SH, Bae BJ, Yang KY, Jeong JH, Kim HS, Lee H. Fabrication of sub-50 nm Au nanowires using thermally curing nanoimprint lithography. *Electron Mater Lett*. 2009;5:139–43. <https://doi.org/10.3365/eml.2009.12.139>.
36. Guo LJ. Nanoimprint lithography: methods and material requirements. *Adv Mater*. 2007;19:495–513. <https://doi.org/10.1002/adma.200600882>.
37. Yoon G, Kim K, Huh D, Lee H, Rho J. Single-step manufacturing of hierarchical dielectric metalens in the visible. *Nat Commun*. 2020;11:1–10. <https://doi.org/10.1038/s41467-020-16136-5>.
38. Yoon G, Kim K, Kim SU, Han S, Lee H, Rho J. Printable nanocomposite metalens for high-contrast near-infrared imaging. *ACS Nano*. 2021;15:698–706. <https://doi.org/10.1021/acsnano.0c06968>.
39. Kim K, Yoon G, Baek S, Rho J, Lee H. Facile nanocasting of dielectric metasurfaces with Sub-100 nm resolution. *ACS Appl Mater Interfaces*. 2019;11:26109–15. <https://doi.org/10.1021/acsami.9b07774>.
40. Greiner C, Del Campo A, Arzt E. Adhesion of bioinspired micropatterned surfaces: effects of pillar radius, aspect ratio, and preload. *Langmuir*. 2009;23:3495–502. <https://doi.org/10.1021/la0633987>.
41. Brörmann K, Burger K, Jagota A, Bennewitz R. Discharge during detachment of micro-structured PDMS sheds light on the role of electrostatics in adhesion. *J Adhes*. 2012;88:589–607. <https://doi.org/10.1080/00218464.2012.682897>.
42. Mukherjee R, Patil GK, Sharma A. Solvent vapor-assisted imprinting of polymer films coated on curved surfaces with flexible PVA stamps. *Ind Eng Chem Res*. 2009;48:8812–8. <https://doi.org/10.1021/ie801740y>.
43. Schaper CD, Miahnahri A. Polyvinyl alcohol templates for low cost, high resolution, complex printing. *J Vac Sci Technol B*. 2004;22:3323–6. <https://doi.org/10.1116/1.1827218>.
44. Hwang SY, Hong SH, Jung HY, Lee H. Fabrication of roll imprint stamp for continuous UV roll imprinting process. *Microelectron Eng*. 2009;86:642–5. <https://doi.org/10.1016/j.mee.2008.11.05542>.
45. Qin D, Xia Y, Whitesides GM. Soft lithography for micro- and nanoscale patterning. *Nat Protoc*. 2010;5:491. <https://doi.org/10.1038/nprot.2009.234>.
46. Delamarche E, Schmid H, Michel B, Biebuyck H. Stability of molded polydimethylsiloxane microstructures. *Adv Mater*. 1997;9:741–6. <https://doi.org/10.1002/adma.19970090914>.
47. Jung GY, Li Z, Wu W, Chen Y, Olynick DL, Wang SY, Tong WM, Williams RS. Vapor-phase self-assembled monolayer for improved mold release in nanoimprint lithography. *Langmuir*. 2005;21:1158–61. <https://doi.org/10.1021/la0476938>.
48. Shen F, Wang A. Fast-fourier-transform based numerical integration method for the rayleigh-sommerfeld diffraction formula. *Appl Opt*. 2006;45:1102–10. <https://doi.org/10.1364/AO.45.001102>.
49. Kim J, Seong J, Kim W, Lee GY, Kim S, Kim H, Moon SW, Oh DK, Yang Y, Park J, Jang J, Kim Y, Jeong M, Park C, Choi H, Jeon G, Lee Ki, Yoon DH, Park N, Lee B, Lee H, Rho J. Scalable manufacturing of high-index atomic layer-polymer hybrid metasurfaces for metaphotonics in the visible. *Nat Mater*. 2023;22:474–81.
50. Choi KM, Rogers JA. A photocurable poly (dimethylsiloxane) chemistry designed for soft lithographic molding and printing in the nanometer regime. *J Am Chem Soc*. 2003;125:4060–1. <https://doi.org/10.1021/ja029973k>.
51. Ulman A. Formation and structure of self-assembled monolayers. *Chem Rev*. 1996;96:1533–54. <https://doi.org/10.1021/cr9502357>.
52. Schreiber F. Structure and growth of self-assembling monolayers. *Prog Surf Sci*. 2000;65:151–257.[https://doi.org/10.1016/S0079-6816\(00\)00024-1](https://doi.org/10.1016/S0079-6816(00)00024-1).

Publisher's Note

Springer Nature remains neutral with regard to jurisdictional claims in published maps and institutional affiliations.

Submit your manuscript to a SpringerOpen[®] journal and benefit from:

- Convenient online submission
- Rigorous peer review
- Open access: articles freely available online
- High visibility within the field
- Retaining the copyright to your article

Submit your next manuscript at ► [springeropen.com](https://www.springeropen.com)
